This paper appears in Control Engineering Practice, 2015.
http://dx.doi.org/10.1016/j.conengprac.2015.03.004

Available online at www.sciencedirect.com

ScienceDirect

Control Engineering Practice 00 (2015) 1–28

Control Engineering Practice

Bilateral Teleoperation System Stability with Non-passive and Strictly-Passive Operator or Environment

Ali Jazayeri and Mahdi Tavakoli *

Department of Electrical and Computer Engineering, University of Alberta, Edmonton, AB T6G 2V4, Canada
Email: ali.jazayeri@ualberta.ca, tavakoli@ece.ualberta.ca

Abstract

A bilateral teleoperation system comprises a human operator, a teleoperator, and an environment. Without exact models for the teleoperator's terminations (i.e., human operator and the environment), it is typically assumed that they are passive but otherwise arbitrary. Based on this assumption, the stability of the teleoperation system is investigated through Llewellyn's absolute stability criterion for the teleoperator. However, the assumption of passivity of the terminations is less than accurate and may be violated in practice. Using Mobius transformations, this paper develops a new powerful stability analysis tool for a two-port network coupled to a passive termination and another termination that is (a) input strictly-passive (ISP), (b) output strictly-passive (OSP), (c) input non-passive (INP), or (b) disc-like non-passive (DNP). While this new stability criterion is applicable to any two-port network, we apply it to bilateral teleoperation systems with position-error-based (PEB) and direct-force-reflection (DFR) controllers. Simulations and experiments are reported for a pair of Phantom haptic robots.

Keywords: Teleoperation Systems, Absolute stability, Non-passive termination, Strictly passive termination, Llewelly's criterion

Abbreviations

LTI	Linear time-invariant
PEB	Position error based
DFR	Direct force reflection
DFR(PD)	Force-position with PD position controller
DFR(P+D)	Force-position with P+D position controller
RHP	Right half plane
LHP	Left half plane

*Corresponding author

ISP	Input strictly-passive
OSP	Output strictly-passive
INP	Input non-passive
ONP	Output non-passive
DNP	Disc-like non-passive
EOP	Excess of passivity
SOP	Shortage of passivity
OER	Operator emulating robot

Nomenclature

f_m	Control signal for the master
f_s	Control signal for the slave
f_h	Operator's force
f_e	Environment's force
x_m	Master position
x_s	Slave position
$C_m(s)$	Position controller for master
$C_s(s)$	Position controller for slave
k_{p_m}, k_{v_m}	Proportional and derivative gains of C_m
k_{p_s}, k_{v_s}	Proportional and derivative gains of C_s
Z_m	Impedance of the master
Z_s	Impedance of the slave
μ	Position scaling factor
λ	Force scaling factor
α	Ratio $C_m(s)/C_s(s)$
β	Initial energy of a passive system
δ	EOP of an ISP system
ϵ	EOP of an OSP system
η	SOP of an INP system
υ	SOP of an ONP system
ρ	SOP of a DNP system
Z_{ij}	The i-th row and j-th column element of an impedance matrix

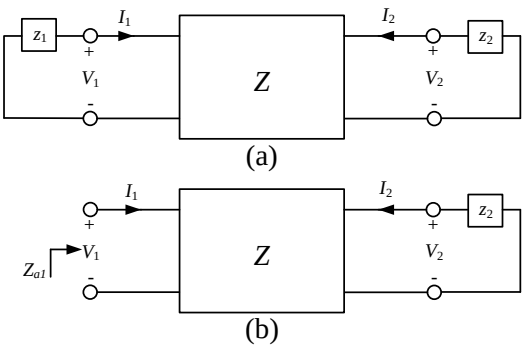

Figure 1. (a) A two-port network connected to two one-port network terminations, and (b) the driving-point impedance at port 1, $Z_{a1} = V_1/I_1$, when port 2 is terminated to a passive impedance z_2.

R_{ij} Real part of Z_{ij}

I_{ij} Imaginary part of Z_{ij}

z_2 Impedance coupled to port 2 of a two-port network

Z_{a1} Driving-point impedance at port 1 of a two-port network

A, B, C Parameters of a generalized circle in the complex plane

1. Introduction

Stability analysis of a bilateral teleoperation system is challenging due to two typically unknown elements in its two ends: the human operator and the environment Hannaford and Wood (1989); Yan and Salcudean (1996); Hokayem and Spong (2006). For analysis of stability, a teleoperation system is typically modeled as a two-port network teleoperator connected to the two one-port network terminations (Fig. 1-a), where the teleoperator comprises the master, the slave, their controllers, and the communication channel and the terminations are the human operator and the environment. By definition, absolute stability of a two-port network will guarantee the stability of the coupled system resulting from connecting the two-port network to two passive but otherwise arbitrary one-port network terminations. Equivalently, two-port network absolute stability requires that the driving-point impedance seen at one of the ports is passive when the other port is terminated to a passive one-port network (Fig. 1-b) Haykin (1970). Therefore, the notion of absolute stability has been applied to the stability analysis of coupled two-port networks with limited information about the terminations.

1.1. Llewellyn's absolute stability criterion

For stability analysis of a bilateral teleoperation system, sometimes the passivity of the teleoperator is investigated Anderson and Spong (1989); Lee and Spong (2006); Niemeyer and Slotine (2004); Nuno et al. (2011), which is sufficient for its absolute stability Haykin (1970). The teleoperator's absolute stability is a less conservative condition compared to its passivity. Due to stability-transparency trade-offs in a bilateral teleoperation system, minimizing conservatism in stability analysis is important Lawrence (1993); Li et al. (2013); Kim et al. (2013).

A well-known absolute stability criterion for two-port networks was proposed by Llewellyn Llewellyn (1952) and applied to bilateral teleoperators Adams and Hannaford (1999); Hashtrudi-Zaad and Salcudean (2001); Aziminejad et al. (2008). Llewellyn's absolute stability criterion gives closed-form conditions involving the immittance (impedance, admittance, hybrid, and transmission, Aliaga et al. (2004)) parameters of a two-port network for it to be absolutely stable Haykin (1970); Ku (1963).

1.2. Assumption on termination passivity

Llewellyn's absolute stability criterion requires both of the terminations of the two-port network to be passive. Passivity of a linear time-invariant (LTI) system is equivalent to the positive-realness of its input-output relationship in the frequency domain (transfer function or impedance in the context of this paper) Marquez (2003). Equivalently, a passive LTI system has an impedance with its Nyquist diagram entirely in the right half of the complex plane (RHP).

Expecting the passivity of both of the terminations of a teleoperation system can be unrealistic and overly restrictive in some applications. A two-port network's termination may simply be non-passive Hirche et al. (2009); Matiakis et al. (2009). On the other hand, a termination can be strictly-passive. Later in the paper, we will discuss specific examples of such terminations for bilateral teleoperation systems. In this paper, a powerful tool is developed for stability analysis of a two-port network coupled to a passive termination and a non-passive or strictly-passive termination with certain constraints on the termination's impedance.

Interestingly, to have a stable coupled system, it suffices if, after terminating the two-port network to a one-port network that is not necessarily passive, the driving-point impedance seen at the remaining (i.e., open) port is passive. This is because connecting a passive termination at the currently open port of this two-port network will inevitably result in a passive and thus stable system even though the opposite port might have been connected to a non-passive termination. As we will see later, this can be explained by the concepts of excess of passivity (EOP) and shortage of passivity (SOP) for feedback-interconnected systems. Briefly, when two systems are connected in a negative feedback loop, the stability of the interconnected system is guaranteed if both systems are passive. If one of the system has EOP, the other system may have SOP without risking the instability of the interconnected system Sepulchre et al. (2012).

1.3. Leveraging termination knowledge in stability analysis

Utilizing knowledge about a termination in the analysis of stability of a coupled two-port network has been increasingly investigated by researchers. For instance, knowing a lower or upper bound on the impedance of a termination helps to model the termination as an arbitrary impedance coupled to a series or shunt impedance, respectively Hashtrudi-Zaad and Salcudean (2001); Adams and Hannaford (2002). In another work, notion of bounded impedance absolute stability (BIAS) is applied to a teleoperation system in the scattering domain and the resulted stability conditions are expressed as bounds on the reflection coefficients Haddadi and Hashtrudi-Zaad (2012). The teleoperation system can be modeled in the integral quadratic constraints (IQC) formulation to reestablish stability conditions with known bounds on the termination Polat and Scherer (2012).

Also, recent work shows that conventional absolute stability criteria can be extended to strictly-passive Jazayeri and Tavakoli (2012b) and non-passive terminations Jazayeri et al. (2013).

In recent works, stability analysis of two-port network systems have been studied when the terminations are either ISP or INP. In Jazayeri and Tavakoli (2012b) two approaches are applied to extend Llewellyns absolute stability. In the first approach, the driving point impedance at port 1 is assumed to be in the RHP and the admissible Nyquist region for termination 2 is found. In the second approach, port 2 is assumed to be a right- or left-shifted RHP and the resulting driving-point impedance at port 1 becomes a disc, which should be entirely in the RHP for stability of the coupled two-port network. In Jazayeri et al. (2013), the second approach is applied when the terminations are non-passive rectangular impedance or right-shifted RHP impedances. In both above work, the stability analysis is applied to a PEB-controlled bilateral teleoperation systems. This paper leverages the second approach when the terminations are INP/ISP/ONP/DSP/OSP and applies the results to PEB- and DFR-controlled bilateral teleoperation systems. In addition, this paper verifies the resulting stability conditions in simulations and experiments with operator-Emulating-Robot (OER).

1.4. Examples of non-passive and strictly-passive terminations

For a human operator, non-passivity may occur in many cases Chopra et al. (2008); Rodriguez-Seda and Spong (2009). On the other hand, a typical environment may be strictly-passive in many applications. Examples of these are given below.

Let us consider an example of a non-passive termination in a master-slave teleoperation system. When the master is manipulated by a human operator, the operator is typically assumed to be passive. This assumption is valid for tasks that involve a relaxed arm such as sensing (or relaxed grasp) tasks Hogan (1989); Dyck et al. (2013). However, the human operator is non-passive in many other practical cases including in posture-maintenance (i.e., rigid grasp) tasks Dyck et al. (2013) or trajectory following tasks Jazayeri et al. (2013). This is intuitively understood by considering a teleoperator that has been designed to be passive. The interconnection of this passive teleoperator and a passive environment will be passive van der Schaft (1999). Therefore, the only source of net energy in the system can be the human operator. If the human operator is also passive, no active motion can exist in the system. Thus, the human operator must be generating energy, e.g., when following a trajectory. Another example of a non-passive termination in a teleoperation system is a non-passive environment. This happens when external forces such as gravity enable the environment to do work on the teleoperator. As another example, a beating heart in a surgical teleoperation system is an environment that emits energy.

In another example, let us consider a teleoperation system with a strictly-passive termination. A mass-spring-damper system is output strictly-passive with excess of passivity equal to the system damping. In general, in the presence of viscous friction (i.e., damping) an otherwise passive environment becomes strictly-passive.

1.5. Methodology

In this paper, a stability analysis tool is developed to investigate the stability of a two-port network coupled to a passive termination and either (a) a strictly-passive termination or (b) a non-passive termination. Llewellyn's absolute stability criterion is derived as a special case of the proposed stability criterion. While a passive impedance has a Nyquist diagram in the RHP, the Nyquist diagram of a strictly-passive impedance is placed only in a subset of the RHP. Conversely, the Nyquist diagram of a non-passive impedance trespasses the jω-axis and into the left half of the complex plane (LHP).

Input strictly-passive (ISP) and output strictly-passive (OSP) systems have Nyquist diagrams inside a right-shifted RHP and a disc to the right of and tangent to the origin, respectively Lozano et al. (2007); Hill and Jensen (1998). The borderlines of these regions are expressed by lines or circles in the complex plane. Similar to ISP and OSP systems, their non-passive counterparts are defined as input non-passive (INP) and output non-passive (ONP) systems with Nyquist diagrams inside a left-shifted RHP and a disc to the left of and tangent to the origin, respectively. Since the notion of ONP does not correspond to useful physical systems, a more useful alternative is defined as a disc-like non-passive (DNP) system whose Nyquist diagram is placed inside a disc centered at the origin. The stability criterion proposed in this paper applies to a two-port network connected to a passive termination and to another termination that is ISP, OSP, INP or DNP.

A mass-damper-spring system with force input and velocity output is an example of OSP systems and a lead-lag controller is an example of ISP systems. In order to determine if a given linear time-invariant system is ISP, OSP, INP or DNP one can plot the Nyquist diagram of its transfer function.

A human operators impedance (with velocity input and force output) is a DNP system for the following reason. The human arm impedance's magnitude has an upper bound depending on the muscle strength and arm configuration. As shown in Dyck (2013), Dolan et al. (1993) and Tsuji et al. (1995), the impedance of the human operator's arm is shown to be inside an impedance ellipse in the x-y directions. As a result, in either of x or y directions (please remember that our paper deals with a 1-DOF model of the human operators impedance), there is an upper bound on the arm impedance while the impedance phase can vary. As shown in Section 2, this upper bound is the radius of the DNP impedance disk in Fig. 2-f. This justifies why the human arm is modeled as the DNP impedance in Fig. 2-f. Boundedness of the human operator impedance can be verified through its physical interpretation. Impedance by its definition is the mapping from the force input to the velocity output for various frequencies. As shown in Dyck (2013), Dolan et al. (1993) and Tsuji et al. (1995), the human arm impedance can be modeled as a mass-spring-damper system. The Nyquist plot of such a second-order system system will necessarily be bounded because the damping term is not zero.

1.6. Advantages of the proposed stability criterion

Taking into account the SOP of a non-passive termination as proposed in this paper will allow to predict the potential instability of a coupled two-port network where the conventional absolute stability conditions fails to do so. Also, the proposed stability criterion will help ensure the stability of a coupled two-port network terminated to a non-passive termination by choosing the controllers gains in a more stringent fashion compared to the conventional absolute stability condition. On the other hand, taking into account the EOP of a strictly-passive termination as proposed in this paper will enable us to reduce conservatism in controller design and potentially enhance teleoperation performance compared to when the conventional absolute stability condition is used. In fact, strict-passivity of the terminations allows having a non-passive teleoperator while preserving coupled stability, which can help to improve performance.

1.7. Organization of the paper

The paper is organized as follows. First, mathematical background and definitions are presented in Section 2. In Section 3, Mobius transformations of regions in the complex plane are applied to find stability condition when a termination is ISP, OSP, INP, or DNP. While the results of Section 3 are applicable to any two-port network, an important application of the new conditions is in bilateral teleoperation systems discussed in Section 4. A simulation study for a teleoperation system is presented in Section 5. In Section 6, the experimental results are presented for a teleoperation system. Finally, concluding remarks and future work are presented in Section 7.

2. Mathematical Preliminaries

This section includes definitions and prerequisite theories that are used in the subsequent sections. Notions of passivity, absolute stability, positive realness, and strict-passivity are defined below. In the paper, all the units are in SI unless specified otherwise.

Notation:

- $\mathbf{A}$, a and $A(s)$ denote a matrix, a scalar and a variable in Laplace domain, respectively. Complex conjugate of a is denoted by $\bar{a}$.
- A circle in the complex plane is expressed as $\mathcal{C}(r, c)$, where $r \in \mathbb{R}$ is the radius and $c \in \mathbb{C}$ is the centre of the circle. The area inside this circle is denoted by the disc $\mathcal{D}(r, c)$.

Assumptions:

- The dynamics of the master and slave robots are LTI and known [2].
- The dynamics of the human operator and the environment are LTI but not necessarily known.
- The communication link between the master and the slave has negligible time-delay.

2.1. Definitions of passivity and absolute stability

Definition 1. *Lozano et al. (2007); Sepulchre et al. (2012) A system with input $u(.)$ and output $y(.)$ where $u(t), y(t) \in \mathbb{R}^m$ is passive if there is a constant β such that*

$$\int_0^t y^T(\tau)u(\tau)d\tau \geq \beta \tag{1}$$

for all functions $u(.)$ and all $t \geq 0$. The constant β is the energy stored in the system at time $t = 0$.

[2] Feedback linearization (inverse dynamics) approach converts the nonlinear and coupled dynamics of an n-DOF robot to a decoupled, LTI system Spong and Vidyasagar (2008); Isidori (1999).

Definition 2. *Lozano et al. (2007); Hill and Moylan (1977) A system with input $u(.)$ and output $y(.)$ where $u(t), y(t) \in \mathbb{R}^m$ is ISP if there are constants β and $\delta > 0$ such that*

$$\int_0^t y^T(\tau)u(\tau)d\tau \geq \beta + \delta \int_0^t u^T(\tau)u(\tau)d\tau \tag{2}$$

for all functions $u(.)$ and all $t \geq 0$. The value δ is the EOP for the ISP system.

Definition 3. *Lozano et al. (2007) A system with input $u(.)$ and output $y(.)$ where $u(t), y(t) \in \mathbb{R}^m$ is OSP if there are constants β and $\epsilon > 0$ such that*

$$\int_0^t y^T(\tau)u(\tau)d\tau \geq \beta + \epsilon \int_0^t y^T(\tau)y(\tau)d\tau \tag{3}$$

for all functions $u(.)$ and all $t \geq 0$. The value ϵ is the EOP for the OSP system.

Definition 4. *In Definition 2, if $\delta < 0$, the system is INP with SOP of $\eta = -\delta$.*

Definition 5. *In Definition 3, if $\epsilon < 0$, the system is ONP with SOP of $\upsilon = -\epsilon$.*

Instead of ONP systems in Definition 5, we define a more useful class corresponding to DNP systems as below.

Definition 6. *An LTI system $G(s)$ is DNP with SOP of ρ if $|G(j\omega)| \leq 1/2\rho$.*

Definition 7. *Khalil (2001) A $p \times p$ proper rational transfer function matrix $G(s)$ is positive real if*

- *all poles of all elements of $G(s)$ meet $\mathrm{Re}\{s\} \leq 0$,*
- *any pure imaginary pole $j\omega$ of any element of $G(s)$ is a simple pole and the residue matrix $\lim_{s\to\infty}(s - j\omega)G(s)$ is positive semidefinite Hermitian.*
- *for all real ω for which $j\omega$ is not a pole of any element of $G(s)$, the matrix $G(j\omega)+G^T(-j\omega)$ is positive semidefinite.*

2.2. Lemmas of passivity and absolute stability

For a scalar rational transfer function, the last part of Definition 7 reduces to $\mathrm{Re}\, G(j\omega) \geq 0$. The following lemma establishes the connection between passivity of a transfer function and the region covered by its Nyquist diagram in the complex plane.

Lemma 1. *Lozano et al. (2007); Slotine and Li (1991) Consider an LTI rational transfer function $G(s)$. Assume that all poles of $G(s)$ have negative real parts. The system is passive if and only if $\mathrm{Re}G(j\omega) \geq 0$ for all frequencies ω (Fig. 2-a).*

Similarly, Lemmas 2-3 below make the connection between EOP of ISP and OSP systems to the corresponding Nyquist diagram regions in the complex plane.

Lemma 2. *Lozano et al. (2007) Consider an LTI rational transfer function $G(s)$. Assume that all poles of $G(s)$ have negative real parts. The system is ISP with EOP of δ if and only if $\mathrm{Re}G(j\omega) \geq \delta$ for all frequencies ω (Fig. 2-b).*

Lemma 3. *Lozano et al. (2007) Consider an LTI rational transfer function $G(s)$. Assume that all poles of $G(s)$ have negative real parts. The system is OSP with EOP of ϵ if and only if the Nyquist diagram of $G(j\omega)$ is contained in the disc $\mathcal{D}(1/(2\epsilon), 1/(2\epsilon))$ for all frequencies ω (Fig. 2-c), i.e., $\mathrm{Re}G(j\omega) \geq \epsilon|G(j\omega)|^2$.*

Dual to the EOP of an ISP system (Lemma 2), we can relate the SOP of an INP system to its Nyquist diagram region. For example, if $G(s)$ is an INP system with SOP of η, then $\mathrm{Re}G(j\omega) \geq -\eta$ (Fig. 2-d).

Passivity has been vastly used in the teleoperation literature to ensure stability. The connection between passivity and absolute stability is made via the following lemma.

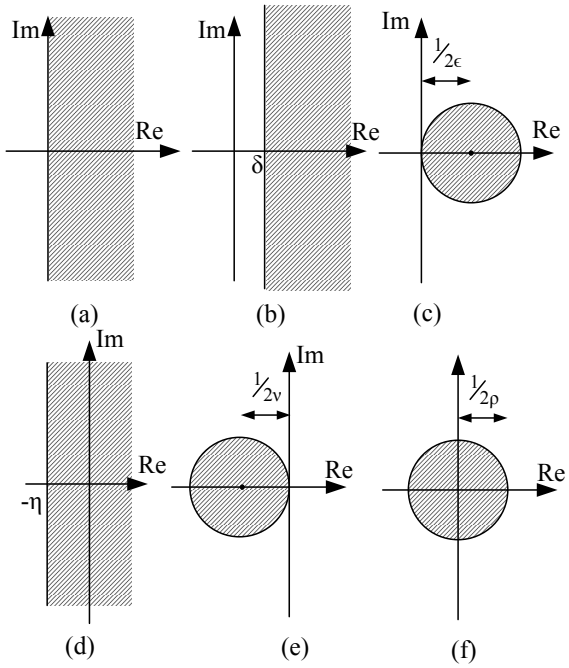

Figure 2. Nyquist diagrams of (a) a passive system, (b) an ISP system with EOP of δ, (c) an OSP system with EOP of ϵ, (d) an INP system with SOP of η, (e) an ONP system with SOP of υ, (f) a DNP system with SOP of ρ.

Lemma 4. *A two-port network is absolutely stable if and only if for any passive but otherwise arbitrary termination of a port, the driving-point impedance at the other port is passive.*

Lemma 5. *In the complex plane of z, a line and a circle are expressed by the following unified formulation:*

$$Az\bar{z} + \bar{B}z + B\bar{z} + C = 0 \tag{4}$$

where $A, B, C \in \mathbb{C}$ are the parameters of the circle or the line. If $A = 0$, (4) reduces to the equation of a line. If $A \neq 0$, (4) expresses the following circle Levinson and Redheffer (1970):

$$\mathcal{C}(\frac{\sqrt{|B|^2 - AC}}{|A|}, -B/A) \tag{5}$$

3. Main results

Mappings of the regions in the impedance plane are introduced in Section 3.1. In Section 3.2 and Section 3.3, these mappings will be applied to find stability conditions for a two-port network with a non-passive and strictly-passive terminations, respectively.

3.1. Mapping of regions via Mobius transformation

A two-port network is expressed by its impedance Z matrix as

$$\begin{bmatrix} V_1(s) \\ V_2(s) \end{bmatrix} = \begin{bmatrix} Z_{11}(s) & Z_{12}(s) \\ Z_{21}(s) & Z_{22}(s) \end{bmatrix} \begin{bmatrix} I_1(s) \\ I_2(s) \end{bmatrix} \tag{6}$$

where the pairs (V_1,V_2) and (I_1,I_2) denote the voltages and currents at the two terminals. When port 2 is connected to a termination with impedance z_2 (Fig. 1-b), the driving-point impedance Z_{a1} at port 1 is expressed as

$$Z_{a1} = Z_{11} - \frac{Z_{12}Z_{21}}{Z_{22} + z_2} = \frac{z_2(Z_{11}) + (Z_{11}Z_{22} - Z_{12}Z_{21})}{z_2 + (Z_{22})} \tag{7}$$

In the following, the result of mapping two general areas representing the impedance z_2 – a rectangle and a disk – will be found in the Z_{a1} impedance plane.

3.1.1. Mapping of a rectangular impedance via Mobius transformation

In order to investigate the stability of a two-port network with ISP or INP terminations, we introduce the following theorem to study the mappings of such terminations.

Theorem 1. *Suppose that the termination z_2 has a rectangular shape in the complex impedance plane, namely $-a \leq \mathrm{Re} z_2 \leq b$, $-d \leq \mathrm{Im} z_2 \leq c$ as shown in Fig. 3-a. This region in the z_2 plane is mapped by the Mobius transformation (7) to a crescent-like region in the Z_{a1} plane defined by the outer circle*

$$\mathcal{C}\left(\frac{|Z_{12}Z_{21}|}{2(R_{22}-a)}, Z_{11}-\frac{Z_{12}Z_{21}}{2(R_{22}-a)}\right) \tag{8}$$

and the inner circle

$$\mathcal{C}\left(\frac{|Z_{12}Z_{21}|}{2(R_{22}+b)}, Z_{11}-\frac{Z_{12}Z_{21}}{2(R_{22}+b)}\right) \tag{9}$$

after excluding the following two discs:

$$\mathcal{D}\left(\frac{|Z_{12}Z_{21}|}{2c+2I_{22}}, \frac{Z_{11}+jZ_{12}Z_{21}}{2c+2I_{22}}\right) \tag{10}$$

$$\mathcal{D}\left(\frac{|Z_{12}Z_{21}|}{2d+2I_{22}}, \frac{Z_{11}+jZ_{12}Z_{21}}{-2d+2I_{22}}\right) \tag{11}$$

□

The mapped region in the Z_{a1} plane is shown in Fig. 3-b. Proof of Theorem 1 is given in Appendix Appendix A.

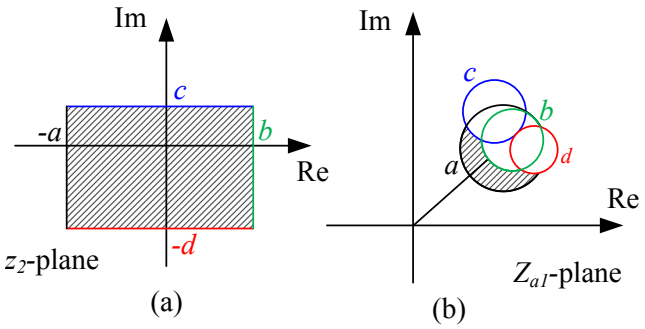

Figure 3. A rectangle in the z_2-plane (a) is transformed into the hatched region in the Z_{a1}-plane (b). The circles are marked in relation with the corresponding lines.

Remarks:

- The circles shown in Fig. 3 resemble a rotated and translated Smith Chart, which has been applied to investigating the stability of a bilateral teleoperation via reflection coefficients Haddadi and Hashtrudi-Zaad (2010).
- By increasing the parameters a, b, c and d in Fig. 3-a, the outer circle of the crescent in Fig. 3-b enlarges, the inner circle shrinks, and the two discs on the top and bottom shrink.

3.1.2. Mapping of a disc impedance via Mobius transformation

In order to investigate the stability of two-port networks with DNP or OSP terminations, we introduce the following two theorems to study mappings of such terminations.

Theorem 2. *Suppose that the termination impedance z_2 is a disc defined by $\mathcal{D}(M,0)$. This region is mapped by the Mobius transformation (7) to the following region in the Z_{a1}-plane:*

$$\begin{cases} \mathcal{D}(\dfrac{|Z_{12}Z_{21}|M^2}{||Z_{22}|^2-M^2|}, \dfrac{-Z_{22}Z_{12}Z_{21}}{|Z_{22}|^2-M^2}+Z_{11}), \text{ if } |Z_{22}|\neq M. \\ \mathrm{Re}Z_{a1} > \left(R_{11}-\dfrac{\mathrm{Im}\{Z_{12}Z_{21}\}}{2R_{22}}\right), \text{ if } |Z_{22}|=M,\ Z_{22}\in\mathbb{R} \end{cases} \tag{12}$$

□

Proof of Theorem 2 is given in Appendix Appendix A.

While Theorem 2 finds the transformation of a disc-like region (corresponding to a DNP termination), the following theorem finds the transformation if the disc is shifted to the right by M (corresponding to an OSP termination).

Theorem 3. *Consider a Mobius transformation of (7). A disc in the z_2-plane inside of $\mathcal{C}(M,M)$ is mapped by the Mobius transformation (7) to the following region in the Z_{a1}-plane:*

$$\begin{cases} \mathcal{D}(\dfrac{|Z_{12}Z_{21}|M^2}{||Z_{22}+M|^2-M^2|}, \dfrac{-Z_{22}Z_{12}Z_{21}}{|Z_{22}+M|^2-M^2}+Z_{11}), \\ \qquad\qquad \text{if } |Z_{22}+M|\neq M. \\ \mathrm{Re}Z_{a1} > \left(R_{11}-\dfrac{\mathrm{Im}\{Z_{12}Z_{21}\}}{2(R_{22}+M)}\right), \text{ if } |Z_{22}|=M,\ Z_{22}\in\mathbb{R} \end{cases} \tag{13}$$

□

Proof of Theorem 3 is similar to the proof of Theorem 2 and is omitted for brevity.

3.2. Stability of a two-port network with non-passive terminations

Shortage of passivity for a termination of a two-port network means that the coupled network may be unstable even if Llewellyn's conditions are met. Therefore, more stringent conditions for stability will be found in this section for two types of non-passive terminations.

3.2.1. Stability of a two-port network with an INP termination

Let us assume that a non-passive termination's impedance covers a rectangular area in the complex plane. If the region is partially in the LHP with bounds on the real and imaginary parts of the complex impedance, the termination is INP. In Theorem 4 below, the absolute stability condition for a two-port network with this INP termination is introduced.

Theorem 4. *Consider the two-port network (6) and assume that, as shown in Fig. 1-b, the driving-point impedance seen from port 1 is Z_{a1} while port 2 of the two-port network is terminated to an impedance z_2. Assume that z_2 is INP with $-a \leq \mathrm{Re}z_2 \leq b$ and $-d \leq \mathrm{Im}z_2 \leq c$ as shown in Fig. 3-a with $a,b,c,d \geq 0$. If port 1 of the two-port network is terminated to a passive impedance, the necessary and sufficient condition for stability of the coupled system comprising the two-port network, the passive termination at port 1, and the INP termination at port 2 is*

(i) *Z_{11} and Z_{22} have no poles in the RHP,*
(ii) *Pure imaginary poles of Z_{11} and Z_{22} are simple and have positive residues, and*

(iii) *For all real positive frequencies* ω,

$$\begin{aligned} R_{11} &\geq 0 \\ R_{22} &\geq a \\ 2R_{11}R_{22} - \mathrm{Re}\{Z_{12}Z_{21}\} - |Z_{12}Z_{21}| - 2R_{11}a &\geq 0 \end{aligned} \tag{14}$$

□

Proof of Theorem 4 is given in Appendix Appendix A.
Remarks:

- The parameters b, c and d do not appear in the stability condition (14) due to the fact that the inner circle and the top and bottom circles in Fig. 3-b are not the source of any constraint when ensuring the passivity (i.e., the positive realness) of the driving-point impedance Z_{a1}. In other words, besides the parameters of the two-port network, stability depends only on the lower limit of the real part of the INP impedance z_2 (i.e., -a) for the two-port network.
- As a special case of Theorem 4, by setting $a = 0$, $b = \infty$, $c = \infty$ and $d = \infty$, the region covered by the impedance z_2 becomes the entire RHP (i.e., all passive impedances). Evidently, when $a = 0$, our stability condition (14) reduces to the well-known Llewellyn's absolute stability criterion for two passive terminations Ku (1963):

$$\begin{aligned} R_{11} &\geq 0 \\ R_{22} &\geq 0 \\ 2R_{11}R_{22} - \mathrm{Re}\{Z_{12}Z_{21}\} - |Z_{12}Z_{21}| \quad &\geq 0 \end{aligned} \tag{15}$$

- The difference between the stability conditions (14) and (15) is in their second and third conditions. As expected, compared to (15), (14) is more stringent because $a \geq 0$ and it provides for stability of the two-port network coupled to an INP termination.
- a is indeed the SOP of the INP termination z_2 according to Definition 4 and the non-passive dual of Lemma 2.

3.2.2. Stability of a two-port network with a DNP termination

In many applications of bilateral teleoperation, the knowledge about the non-passive termination, e.g., human arm, can be translated to a maximum amplitude of its impedance van der Helm et al. (2002); Park et al. (2011). This maximum impedance is the same as the radius of the disc for a DNP termination, which is expressed as $|z_2| \leq M$. Passivity of a two-port network connected to a DNP termination can be studied using the following theorem.

Theorem 5. *Consider the two-port network system (6) and assume that, as shown in Fig. 1-b, the driving-point impedance seen from port 1 is* Z_{a1} *while port 2 of the two-port network is terminated to an impedance* z_2*. Assume that* z_2 *is DNP with* $|z_2| \leq M$*, where* $M > 0$ *is known. If port 1 of the two-port network is terminated to a passive impedance, the necessary and sufficient condition for stability of the coupled system comprising the two-port network, the passive termination at port 1, and the DNP termination at port 2 is*

(i) Z_{11} *and* Z_{22} *have no poles in the RHP,*
(ii) *Pure imaginary poles of* Z_{11} *and* Z_{22} *are simple and have positive residues, and*

(iii) *For all real positive frequencies* ω,

$$\begin{cases} R_{11} \geq 0 \\ R_{22} \geq 0 \\ R_{22}(|Z_{11}|^2 - M^2) - \mathrm{Re}\{Z_{11}Z_{12}Z_{21}\} \\ \qquad - |Z_{12}Z_{21}|M \geq 0, \qquad \textit{if } |Z_{11}| > M. \\ -R_{22}(|Z_{11}|^2 - M^2) + \mathrm{Re}\{Z_{11}Z_{12}Z_{21}\} \\ \qquad - |Z_{12}Z_{21}|M \geq 0, \qquad \textit{if } |Z_{11}| < M. \\ -2R_{22}R_{11} - \mathrm{Re}\{Z_{12}Z_{21}\} \geq 0, \quad \textit{if } Z_{11} = M. \end{cases} \tag{16}$$

□

Proof of Theorem 5 is similar to the proof of Theorem 4 with the difference that the region covered by the non-passive termination is now a disc, which requires using Theorem 2.

3.3. Stability of a two-port network with strictly-passive terminations

Having excess of passivity for a termination of a two-port network allows for more flexible stability conditions. Input and output strict-passivity of a termination are considered separately in the following two subsections.

3.3.1. Stability of a two-port network with an ISP termination

Theorem 6. *Consider the two-port network system (6) and assume that, as shown in Fig. 1-b, the driving-point impedance seen from port 1 is* Z_{a1} *while port 2 of the two-port network is terminated to an impedance* z_2*. Assume that* z_2 *is ISP with* $\mathrm{Re}z_2 \geq \delta \geq 0$*. If port 1 of the two-port network is terminated to a passive impedance, the necessary and sufficient condition for stability of the coupled system comprising the two-port network, the passive termination at port 1, and the ISP termination at port 2 is*

(i) Z_{11} *and* Z_{22} *have no poles in the RHP,*
(ii) *Pure imaginary poles of* Z_{11} *and* Z_{22} *are simple and have positive residues, and*
(iii) *For all real positive frequencies* ω,

$$\begin{aligned} R_{11} &\geq 0 \\ R_{22} &\geq -\delta \\ 2R_{11}R_{22} - \mathrm{Re}\{Z_{12}Z_{21}\} - |Z_{12}Z_{21}| + 2R_{11}\delta \quad &\geq 0 \end{aligned} \tag{17}$$

□

Proof of Theorem 6 is similar to the proof of Theorem 4 with the difference that $\delta = -a$.
Remark:

- The last condition in (17) for coupled stability of a two-port network with an ISP termination can be compared to its non-passive counterpart in (14). It is clear that the latter is more conservative. Intuitively, for coupled stability, the two-port network should absorb more energy when connected to a non-passive termination than when connected to a strictly-passive termination.

3.3.2. Stability of a two-port network with an OSP termination

In many applications of bilateral teleoperation, the only knowledge about the strictly-passive termination is that its Nyquist diagram is a disc that is centered on the positive segment of the real axis and is tangent to the imaginary axis at the origin. This disc can be expressed as $\mathrm{Re}G(j\omega) \geq \epsilon|G(j\omega)|^2$, where ϵ is EOP of the OSP termination. If $\epsilon = 0$, the termination becomes passive as its Nyquist diagram will be in the RHP.

Theorem 7. *Consider the two-port network system (6) and assume that, as shown in Fig. 1-b, the driving-point impedance seen from port 1 is Z_{a1} while port 2 of the two-port network is terminated to an impedance z_2. Assume that z_2 is OSP with $\mathrm{Re} z_2 \geq \epsilon |z_2|^2$, where $\epsilon > 0$ is known. If port 1 of the two-port network is terminated to a passive impedance, the necessary and sufficient condition for stability of the coupled system comprising the two-port network, the passive termination at port 1, and the OSP termination at port 2 is*

(i) *Z_{11} and Z_{22} have no poles in the RHP,*
(ii) *Pure imaginary poles of Z_{11} and Z_{22} are simple and have positive residues, and*
(iii) *For all real positive frequencies ω,*

$$\begin{gathered} R_{11} \geq 0 \\ R_{22} \geq 0 \\ R_{22}(|Z_{11}+M|^2 - M^2) - \mathrm{Re}\{(Z_{11}+M)Z_{12}Z_{21}\} \\ -|Z_{12}Z_{21}|M \geq 0 \\ |Z_{11}+M| > M \end{gathered} \tag{18}$$

□

where $M = 1/(2\epsilon)$. Proof of Theorem 7 is similar to the proof of Theorem 4 with the difference that the region occupied by the Nyquist diagram of the termination is now a disc, which requires using Theorem 3.

4. Application to Bilateral Teleoperation

The coupled stability conditions presented in Sections 3 are valid for any two-port network. In this section, the two-port network is assumed to be a bilateral teleoperator. In this context, the voltage-current pair (V,I) for the impedance matrix (6) is replaced by the force-velocity pair (F,sX). The coupled stability theorems in Section 3 for strictly-passive and non-passive terminations will be applied to a teleoperator coupled with a non-passive human operator and a strictly-passive environment.

4.1. Modelling of bilateral teleoperation systems

For a 1 degree-of-freedom, bilateral teleoperation system, the master and the slave robots are modelled as LTI systems

$$\begin{aligned} sX_m(s) &= \frac{1}{m_m s + b_m}(F_h(s) - F_m(s)) \\ sX_s(s) &= \frac{1}{m_s s + b_s}(F_e(s) - F_s(s)) \end{aligned} \tag{19}$$

Also, the operator and the environment are modeled as

$$F_h(s) = \tilde{F}_h(s) - sZ_h(s)X_m(s) \tag{20}$$
$$F_e(s) = \tilde{F}_e(s) + sZ_e(s)X_s(s) \tag{21}$$

In the above, F, Z and X denote the force, the impedance and the position, respectively. Also, the subscripts h, e, m and s denote the operator, the environment, the master and the slave, respectively. Furthermore, $\tilde{F}$ represents the exogenous force.

Bilateral teleoperation systems with position error based (PEB) and direct force reflecting (DFR) controllers are shown in Fig. 4. For the PEB architecture, the teleoperation controllers and the impedance matrix of the teleoperator are shown in Table 1, where $F_{m,s}$ are the controller outputs. In this case, the controllers of the master and the slave are $C_s(s) = k_{p_s}/s + k_{v_s}$ and $C_m(s) = k_{p_m}/s + k_{v_m}$, respectively,

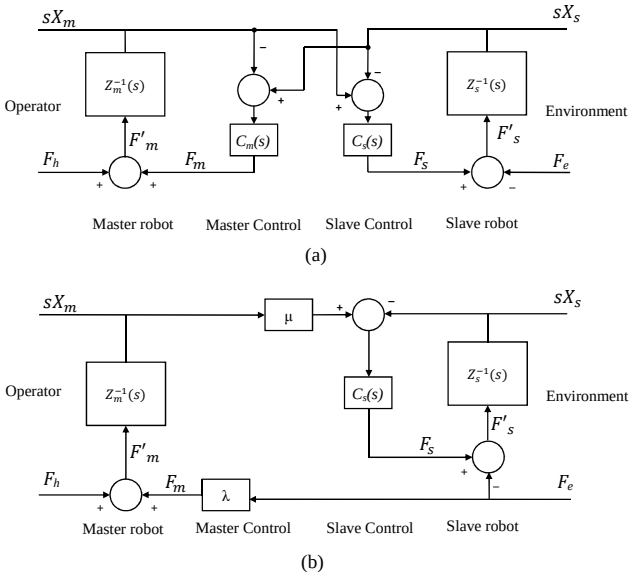

Figure 4. A bilateral teleoperation system, (a) with PEB control, and (b) DFR control.

where $k_{v_m}, k_{v_s}, k_{p_m}, k_{p_s} \geq 0$. For the DFR architecture, the slave robot's position controller may be PD[3] (named DFR(PD) architecture) or P+D (named DFR(P+D) architecture) Willaert et al. (2011). The difference between these two is that position controller for the slave robot; see Table 1. The controllers and the impedance matrices of these two DFR controllers are shown in Table 1, where μ and λ are the position and force scaling factors. Also, $Z_{ts} = Z_s + Cs$ and $Z_{tm} = Z_m + C_m$.

Table 1. Controllers of bilateral teleoperation systems and their impedance matrices

Controller	Control law	Impedance matrix
PEB	$\begin{cases} F_m(s) = C_m(s)(X_s(s) - X_m(s)) \\ F_s(s) = C_s(s)(X_m(s) - X_s(s)) \end{cases}$	$\mathbf{Z_{PEB}} = \begin{bmatrix} Z_{tm} & C_m \\ C_s & Z_{ts} \end{bmatrix}$
DFR(PD)	$\begin{cases} F'_m(s) = F_h(s) - \lambda F_e(s) \\ F'_s(s) = C_s(s)(\mu X_m(s) - X_s(s)) - F_e(s) \end{cases}$	$\mathbf{Z_{PD}} = \begin{bmatrix} Z_m + \mu\lambda C_s & \lambda Z_{ts} \\ \mu C_s & Z_{ts} \end{bmatrix}$
DFR(P+D)	$\begin{cases} F'_m(s) = F_h(s) - \lambda F_e(s) \\ F'_s(s) = k_p(\mu X_m(s) - X_s(s)) - sk_v X_s(s) - F_e(s) \end{cases}$	$\mathbf{Z_{P+D}} = \begin{bmatrix} Z_m + \frac{\mu\lambda k_p}{s} & \lambda Z_{ts} \\ \frac{\mu k_p}{s} & Z_{ts} \end{bmatrix}$

4.2. Teleoperation system stability conditions for passive, INP and ISP terminations

Table 2 compares the necessary and sufficient stability conditions for the PEB, DFR(PD) and DFR(P+D) controlled teleoperation systems when one of the ports is connected a passive, INP or ISP termination. These conditions have resulted from substituting the impedance matrices of PEB, DFR(PD) and DFR(P+D) controlled teleoperation systems from Table 1 into the stability conditions (14), (15) and (17) for INP, passive and ISP terminations, respectively. Derivations of these conditions are omitted for brevity. Note that the position scaling factor μ and the force scaling factor λ appear together in the stability conditions.

Discussions:

[3]Note that the impedance matrix (6) relates velocity to force (instead of position to force); this fact changes the representation of the position controller from PD to PI.

Table 2. Stability conditions for different choices of teleoperation system control architecture and different choice of terminations

Controller	Passive	INP	ISP
PEB	$b_m b_s + b_m k_{v_s} + b_s k_{v_m} \geq \frac{(k_{v_m} k_{p_s} - k_{p_m} k_{v_s})^2}{4 k_{p_m} k_{p_s}}$	$(k_{v_m} + b_m)(b_s - \eta) + b_m k_{v_s} \geq \frac{(k_{v_m} k_{p_s} - k_{p_m} k_{v_s})^2}{4 k_{p_m} k_{p_s}}$ & $b_s + k_{v_s} \geq \eta$	$(k_{v_m} + b_m)(b_s + \delta) + b_m k_{v_s} \geq \frac{(k_{v_m} k_{p_s} - k_{p_m} k_{v_s})^2}{4 k_{p_m} k_{p_s}}$
DFR(PD)	None	None	None
DFR(P+D)	$\mu\lambda \leq \frac{4 b_m}{b_s + k_v}$ & $\mu\lambda \leq \frac{b_m (b_s + k_v)}{m_s k_p}$	$\mu\lambda \leq \frac{4 b_m (b_s + k_v - \eta)}{(b_s + k_v)^2}$ & $\mu\lambda \leq \frac{b_m (b_s + k_v - \eta)}{m_s k_p}$ & $b_s + k_v \geq \eta$	$\mu\lambda \leq \frac{4 b_m (b_s + k_v + \delta)}{(b_s + k_v)^2}$ & $\mu\lambda \leq \frac{b_m (b_s + k_v + \delta)}{m_s k_p}$

- Consider the (PEB, passive) entry of Table 2. The teleoperation system stability requires a lower bound on the robots damping terms b_m and b_s and bounds on the master and slave controllers gains. A sufficient condition for stability of this system is to have the master and the slave controllers proportional to each other:

$$\frac{k_{p_s}}{k_{v_s}} = \frac{k_{p_m}}{k_{v_m}} \tag{22}$$

  The condition (22) is both necessary and sufficient for coupled stability if the master and the slave dynamics only involves masses, i.e., $b_m = b_s = 0$.

- The (PEB, INP) entry of Table 2 is similar to the (PEB, Passive) entry of Table 2 with the exception that b_s is replaced by $b_s - \eta$, where η is the SOP for the INP termination. The physical interpretation of the above fact is that the SOP of the INP termination (connected at port 2) reduces the effective damping of the corresponding robot (the slave robot), which has to be greater than a lower bound in order to ensure stability. In other words, SOP of the INP termination necessitates higher damping for the robot and makes the stability condition harder to satisfy. If the robot damping is not high enough to make up for the SOP of the INP termination, the derivative term of the controllers must be selected high enough to overcome non-passivity of the termination.

- For the (PEB, INP) entry of Table 2, also note that the robot damping terms b_m and b_s cannot be both zero because it causes the left hand side of the first inequality to be negative. This result has an intuitive interpretation. In the (PEB, Passive) case with no damping terms for the master and the slave robots, we saw that the only choice for the controllers was (22). The non-passivity of the termination should make this choice even more limited. However, no freedom is left in the controller parameter space. Therefore, the termination cannot be non-passive.

- The (PEB, ISP) entry of Table 2 is similar to the (PEB, Passive) entry of Table 2 with the exception that b_s is replaced by $b_s + \delta$, where δ is the EOP for the ISP termination. The physical interpretation of the above fact is that the EOP of the ISP termination (connected at port 2) increases the effective damping of the corresponding robot (the slave robot), which has to be greater than a lower bound in order to ensure stability. In other words, EOP of the ISP termination relaxes the lower bound requirement on the robot damping and makes the stability condition easier to satisfy. Also, the robot damping terms b_m and b_s are allowed to be both zero and the controller gain do not necessarily have to be chosen according to (22).

- The INP column of Table 2 includes conditions that are expectedly more limiting than their counterparts in the Passive column. In fact, the more non-passive the termination, the more restrictive the stability condition for the coupled system. Conversely, the ISP column of Table 2 has stability conditions that are less restrictive that their counterparts in the Passive column. In fact, the more passive the termination, the more relaxed the stability condition for the coupled system.

- With the DFR(PD) controller (i.e., force reflection for the master and PD position controller for the slave), substituting the impedance matrix $\mathbf{Z_{PD}}$ into the stability conditions (15), (14) and (17) yields conditions that never hold for $\omega = 0$. This fact has previously been reported in Tavakoli et al. (2007). However, with the DFR(P+D) controller (i.e., force reflection for the master and a P position controller and internal damping for the slave), there does exist a range of controller gains for stability; this has also previously been reported in Willaert et al. (2011). Similar to the PEB controller, in the DFR(P+D) case the effective damping of the robot is reduced or increased by the non-passivity or excess of passivity of the termination, making the stability conditions more restrictive or more relaxed, respectively.

4.3. Teleoperation system stability conditions for DNP and OSP terminations

Substituting the impedance matrices of PEB, DFR(PD) and DFR(P+D) controlled teleoperation systems from Table 1 into the stability conditions of DNP and OSP termination, i.e., (16) and (18), results in conditions of the following form

$$\mathcal{N}(\omega) = N_8\omega^8 + N_6\omega^6 + N_4\omega^4 + N_2\omega^2 + N_0 \geq 0 \tag{23}$$

where N_i's, $i = 0, 2, 4, 6, 8$, are functions of system parameters $m_m, b_m, m_s, b_s, \mu, \lambda, k_v, k_p$ and M. For the DNP termination, $N_0 \geq 0$ corresponding to $\omega = 0$ yields necessary conditions for stability that are shown in Table 3. For the OSP termination, N_0 is always non-negative for PEB, DFR(PD) and DFR(P+D) controllers. Furthermore, in (23), the high frequency component N_8 is non-negative for both DNP and OSP. The terms N_2, N_4 and N_6 may have sign changes depending on the parameters that are involved. Each curve in Fig. 5 indicates the index $\mathcal{N}(\omega)$ for a given M for the condition in the DFR(PD) row of Table 3. For any of the curves of Fig. 5, the condition of stability is that the entire curve is in the non-negative region. This condition is satisfied for $M = 4.8$ but not for $M = 5.1$ because there are some frequencies in the 0-100 rad/sec range where the curve becomes negative and hence the condition in (23) is violated.

Table 3. Necessary conditions for stability of the teleoperation system with DNP termination for PEB, DFR(PD) and DFR(P+D) controllers.

Controller	Condition for having $N_0 \geq 0$
PEB	$M \leq \dfrac{b_s k_{p_m} + b_m k_{p_s} + 2k_{p_s} k_{v_m} + 2k_{p_m} k_{v_s}}{k_{p_s}}$
DFR(PD)	$M \leq b_m + 2\mu\lambda(Bs + 2Kv)$
DFR(P+D)	$M \leq b_m + 2\mu\lambda(Bs + Kv)$

In order to find stability bound, the stability conditions found in Theorems 5 and 7 can be tested over a range of frequencies of interest for a haptic teleoperation system, e.g., 0-100 rad/sec. If the condition $\mathcal{N}(\omega) \geq 0$ is satisfied for the entire range of frequencies, the coupled system is considered stable. An example of the stability index $\mathcal{N}(\omega)$ for the benchmark teleoperator, a DFR(PD) controller, and a DNP termination with various values of disk radius M is plotted in Fig. 5. The parameter of the teleoperation system are $m_m = 0.015$, $b_m = 0.01822$, $m_s = 0.15$, $b_s = 0.1822$, $k_p = 10$, $k_v = 2$ and $\mu\lambda = 0.02$. In this example, the maximum value of disk radius M of the DNP termination is found to be 4.92. Any higher M for the DNP termination can cause instability.

5. Simulation study

A bilateral teleoperation system with PEB control (Fig. 4-a) is simulated in MATLAB/Simulink. Whereas in the experiment in Section 6, we will be limited to having two identical master and slave robots, in the simulations in this section we have the liberty of verifying the proposed stability criteria when the master and the slave robots have different models. The selected model parameters are $m_m = 0.015$ and $b_m = 0.0182$

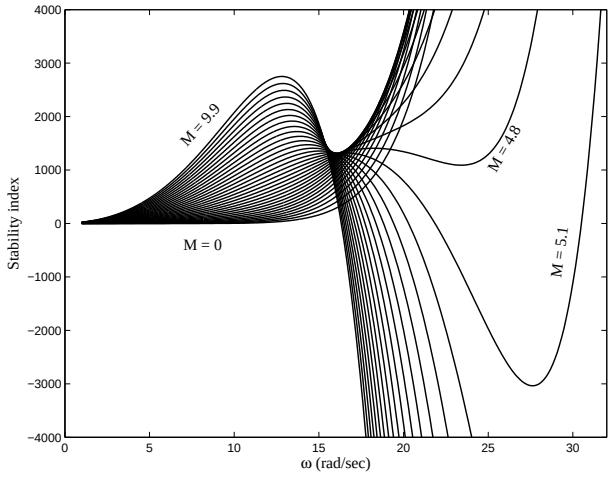

Figure 5. The stability index is evaluated for different values of the disc radius for a range of frequencies.

for the master and $m_s = 0.15$ and $b_m = 0.182$ for the slave. Table 4 compares the theoretical stability conditions (Theory columns) with the simulation results (Simulation Column). In each row of Table 4, the PEB control gains, the operator impedance, and the environment impedance are changed and the robots positions are monitored for boundedness to detect instability. In each Theory column of the table, the theoretical stability conditions in Sections 4.2 and 4.3 are evaluated and the results are listed as either absolutely stable (Abs. Stab.) or potentially unstable (Pot. Unst.).

In Table 4, the terminations are $G_P = \frac{1}{s+1}$, $G_{ISP} = \frac{s+0.5}{s+1}$, $G_{OSP} = \frac{1}{s+1}$, $G_{INP} = \frac{s-0.5}{s+1}$ and $G_{DNP} = \frac{s-1}{s+1}$. The Nyquist diagrams in Fig. 6 show that the EOP values of the ISP and OSP terminations are 0.5 and 1, respectively. Also, the SOP values of the INP and DNP terminations are 0.5 and 0.5, respectively. In all cases, the human operator exogenous force $\tilde{F}_h(s)$ is assumed to be a sine wave with a magnitude of 1 and frequency of 2π rad/sec and the environment exogenous force $\tilde{F}_e(s)$ is assumed to be zero.

Table 4. Comparing stability of teleoperation systems in theory and simulation.

#	Control gains				Terminations		Theory					Simulation
	k_{p_m}	k_{v_m}	k_{p_s}	k_{v_s}	Z_h	Z_e	(PEB, Passive)	(PEB, INP)	(PEB, DNP)	(PEB, ISP)	(PEB, OSP)	
1	10	2	20	2	G_P	G_{OSP}	Abs. Stab.	-	-	-	Abs. Stab.	Stable
2	40	2	10	2	G_P	G_{OSP}	Pot. Unst.	-	-	-	Abs. Stab.	Stable
3	10	1	20	2	G_P	G_{ISP}	Abs. Stab.	-	-	Abs. Stab.	-	Stable
4	20	1	20	2	G_P	G_{ISP}	Pot. Unst.	-	-	Abs. Stab.	-	Stable
5	5	1	20	2	G_{DNP}	G_P	Pot. Unst.	-	Pot. Unst.	-	-	Unstable
6	5	1	20	4	G_{DNP}	G_P	Abs. Stab.	-	Pot. Unst.	-	-	Unstable
7	10	2	40	2	G_{INP}	G_P	Pot. Unst.	Pot. Unst.	-	-	-	Unstable
8	20	2	30	5	G_{INP}	G_P	Abs. Stab.	Pot. Unst.	-	-	-	Unstable

From rows 1 and 3 of the table, we see that if stability in simulations is shown for a set of control gains under the assumption that the terminations are passive, replacing a passive termination with a strictly-passive termination (ISP or OSP) does not alter the result. Conversely, if instability in simulations is shown for a set of control gains under the assumption that the terminations are passive, replacing a passive termination with a non-passive termination may not alter the result; while rows 5 and 7 show two cases of this.

Rows 6 and 8 show that the theoretical stability condition for passive terminations (i.e., Llewellyn's criterion) listed under the column (PEB, passive) expectedly fails to recognize instability if that occurs because of a non-passive termination. Conversely, Rows 2 and 4 show that the theoretical stability condition for passive terminations (i.e., Llewellyn's criterion) listed under the column (PEB, passive) fails to recognize

stability if that occurs because of a strictly-passive termination. In fact, when a termination is strictly-passive, the teleoperation system may be stable even when the teleoperator is recognized by Llewellyn's criterion to be potentially unstable; our proposed stability criterion informs us about this, thus providing an opportunity to leverage higher control gains for improved transparency while preserving stability.

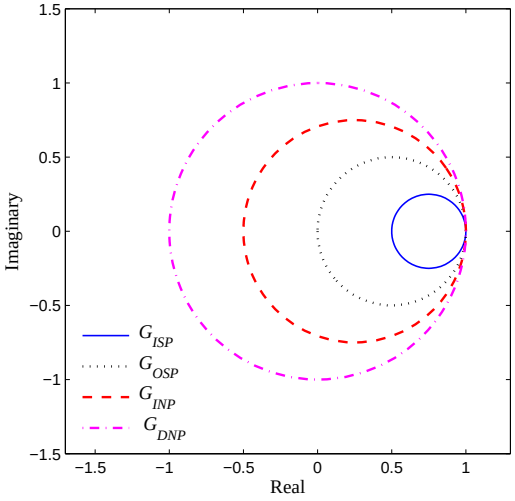

Figure 6. Nyquist diagrams of a ISP, OSP, INP and DNP terminations.

6. Experimental Results

In order to test the stability conditions, experiments are conducted on a pair of Phantom Premium 1.5A haptic devices (Geomagic Inc., Wilmington, MA), which form a bilateral teleoperation system. In the following, two sets of experiments are shown for a strictly-passive termination and a non-passive termination. Typically, it is the environment termination that is strictly-passive while it is the human operator termination that is non-passive.

6.1. Experiments involving a strictly-passive environment

6.1.1. Experimental setup

We use the 1-DOF bilateral teleoperation system shown on Fig. 7 comprising two 3-joint Phantom Premium 1.5A robots as the master and as the slave. The sampling period for the robot is $T_s = 1ms$. In Figure 7, the first joint allows the robot to move the robots end-effector to right and left (x-coordinate). The second joint of the robot moves the end-effector up and down (y-coordinate) and the third joint moves the end-effector in and out (z-coordinate). Out of the three joints of each robot, the first (x) is teleoperated. In this direction, the robot dynamics was identified as a mass-damper with a mass of $m_m = m_s = 0.015$ and a damper of $b_m = b_s = 0.01822$ Jazayeri and Tavakoli (2012a, 2013). The third joint (z) is locked using high-gain control. The second joint (y) is used for a purpose explained below. In the experiments, the environment is designed to be strictly-passive. To design such an environment, the slave robot's end-effector is connected via two springs from opposite sides to a stiff wall and at the same time slides a block of wood on the table. While the spring is passive (lossless), the wood-table viscous friction (acting as a damper) makes the environment strictly-passive. The viscous friction and, therefore, the EOP of the strictly-passive environment can by controlled by changing the perpendicular force, which comes from the robot's second joint (y), on the wood block by the slave robot. In the following experiments, the environment either has a

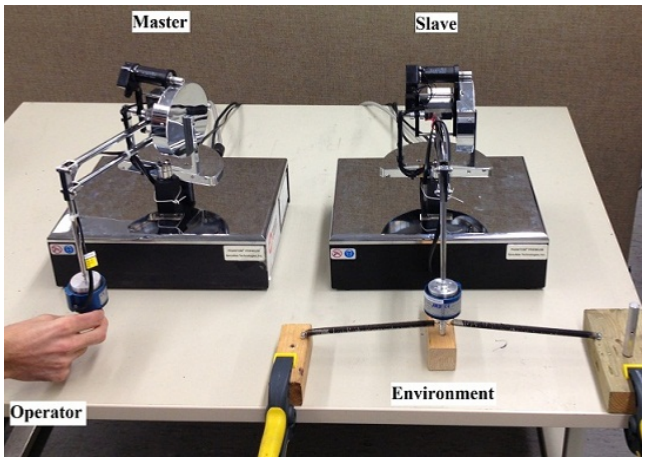

Figure 7. The experimental setup for testing ISP environment.

low EOP ($\tau_y = 0$) or high EOP ($\tau_y = 0.2$ N.m). Using the definition of the EOP (2), in an experiment the values of EOP are identified to be 0.74 and 0.90, respectively. In the following, both PEB (Fig. 4-a) and DFR (Fig. 4-b) controllers are used in the above-mentioned bilateral teleoperation system and in each case the theoretical stability conditions are verified experimentally.

6.1.2. PEB architecture

The bilateral teleoperation system with PEB architecture (Fig. 4-a) is tested for different control gains. The experimentally-obtained positions of the master and the slave are shown in Fig. 8 when the control gains change according to Table 5. The top and the bottom rows of Fig. 8 correspond to EOP values of 0.74 and 0.90 for the ISP environment, respectively.

Figure 8. Master-slave positions for strictly-passive environment with PEB architecture. Top row has $\tau_y = 0$ and and bottom row has torque of $\tau_y = 0.2$ N.m. The controller gains are given in Table 5.

Table 5. Stability condition for the bilateral teleoperation system with PEB controllers

#	Figure	Controller gains				EOP	Theory		Experiment	Tracking Error
		k_{p_m}	k_{v_m}	k_{p_s}	k_{v_s}		(PEB, Passive)	(PEB, ISP)		
1	Fig. 8-a	20	2	30	2	0.74	Pot. Unst.	Abs. Stab.	Stable	0.49858
2	Fig. 8-b	20	2	40	2	0.74	Pot. Unst.	Abs. Stab.	Stable	0.27401
3	Fig. 8-c	1	2	40	2	0.74	Pot. Unst.	Pot. Unst.	Unstable	-
4	Fig. 8-d	20	2	30	2	0.90	Pot. Unst.	Abs. Stab.	Stable	0.70815
5	Fig. 8-e	20	2	40	2	0.90	Pot. Unst.	Abs. Stab.	Stable	0.61674
6	Fig. 8-f	10	2	20	2	0.90	Pot. Unst.	Abs. Stab.	Stable	1.0726

In Table 5, each row shows a selection of control gains for the PEB controller. These controller gains and the robot model have been substituted in the stability conditions of Table 2. In particular, the stability condition in the (PEB, Passive) entry of Table 2 has led to the stability conclusion (i.e., stable or unstable) listed in the (PEB, Passive) column of Table 5. Similarly, the stability condition in the (PEB, ISP) entry of Table 2 has led to the stability conclusion listed in the (PEB, ISP) column of Table 5. Furthermore, the cases of actual instability of the system manifested by growing or sustained oscillations is observed and listed in the Experiment column of Table 5. The last column shows the Euclidean norm of the position tracking error between the master and the slave.

Comparing the controller gains in rows 1 and 2 of Table 5, it is seen that increasing the controller gain k_{p_s} leads to a lower tracking error; in general, as shown in Tavakoli et al. (2007) higher control gains improve performance but undermine the stability of the system. The same phenomenon can be seen when comparing rows 4 and 5. On the other hand, reducing the controller gain k_{p_m} from row 2 to row 3 or from row 5 to row 6 results in an increase in the tracking error.

In all of the 6 experiments of Fig. 8, the conventional (Llewellyn's) stability criterion, i.e., the condition listed in the (PEB, Passive) entry of Table 2, predicts that the teleoperation system is potentially unstable; see the (PEB, Passive) column of Table 5. In practice, however, EOP of the ISP termination causes the teleoperation system to be stable; see the Experiment column of Table 5. This is because the conventional stability condition in the (PEB, Passive) entry of Table 2 is conservative because it guarantees stability of the two-port network for *any* passive termination regardless of its EOP value (which can be as little as zero for a lossless termination). In reality, excess of passivity in a termination allows for tolerating a shortage of passivity in the two-port network such that coupled stability is preserved. Allowing a non-passive two-port network (teleoperator) gives us the flexibility to design less conservative and better performing controllers by increasing the controller gains.

6.1.3. DFR architecture

The bilateral teleoperation system with a DFR architecture (Fig. 4-b) involves a 6-DOF force/torque JR3 force sensor ®(Woodland, CA) and can have different control gains. The force sensor has an internal low-pass filter with a cutoff frequency at 31.25 Hz. Here, a DFR(P+D) controller as described in the last row of Table 1 is used and hence the stability condition in the last row of Table 2 applies. For brevity, the experimentally-obtained positions of the master and the slave are not shown. In Table 6, each row shows a selection of control gains for the DFR(P+D) controller. These controller gains and the robot model have been substituted in the stability conditions of Table 2. In particular, the stability condition in the (DFR(P+D), Passive) entry of Table 2 has led to the stability conclusion (i.e., stable or unstable) listed in the (DFR(P+D), Passive) column of Table 6. Similarly, the stability condition in the (DFR(P+D), ISP) entry of Table 2 has led to the stability conclusion listed in the (DFR(P+D), ISP) column of Table 6. Furthermore, the cases of actual instability of the system manifested by growing or sustained oscillations is observed and listed in the Experiment column of Table 6.

Table 6. Experiments on a teleoperation system with a DFR controller. The scaling factors are $\lambda = 0.2$ and $\mu = 0.5$.

#	Control gains k_p	k_v	EOP	Theory (DFR, passive)	(DFR, ISP)	Experiment
1	10	1	0.74	Pot. Unst.	Abs. Stab.	Stable
2	10	2	0.74	Pot. Unst.	Abs. Stab.	Stable
3	20	2	0.74	Pot. Unst.	Abs. Stab.	Stable
4	20	5	0.74	Pot. Unst.	Abs. Stab.	Stable
5	10	1	0.90	Pot. Unst.	Abs. Stab.	Stable
6	10	2	0.90	Pot. Unst.	Abs. Stab.	Stable
7	20	2	0.90	Pot. Unst.	Abs. Stab.	Stable
8	20	5	0.90	Pot. Unst.	Abs. Stab.	Stable

In Fig. 9, a comparison between DFR(P+D) and DFR(PD) controllers are made. For both controllers, the parameters and gains are EOP = 0.74, $\lambda = 0.5$, $\mu = 1$, $K_p = 20$, and $k_v = 0.1$. In the experiments, the DFR(PD) controller (Fig. 9-a) is unstable while the DFR(P+D) experiment (Fig. 9-b) is stable. This is in agreement with the stability conditions given in the (DFR(P+D), ISP) and (DFR(PD), ISP) entries of Table 2.

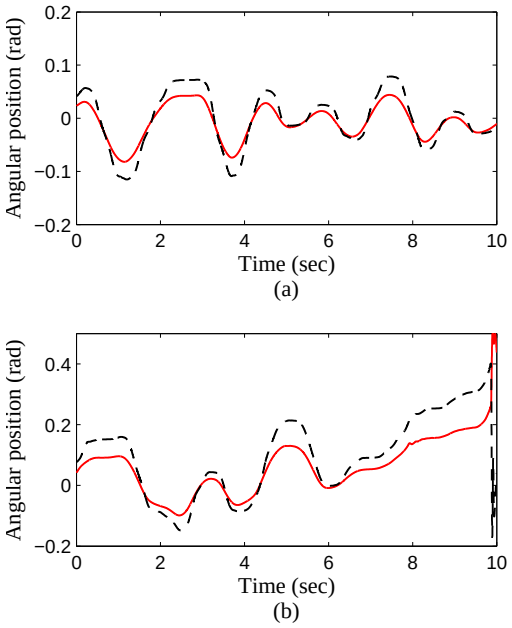

Figure 9. Master-slave positions for an ISP environment in DFR teleoperation with (a) a DFR(P+D) controller, and (b) a DFR(PD) controller.

6.2. Experiments involving a non-passive operator

6.2.1. Experimental setup

Typically, the master is manipulated by a human operator. For reasons described in the following, in this set of experiments, the master is connected to another robot whose task is to manipulate the master. The robot that takes the place of the human operator is called operator emulating robot (OER). Experiments involving a human operator are not easily reproducible due to the fact that every person's arm has a unique physical characteristics. Even for the same human operator, the hand impedance and passivity/activity varies from the beginning to the end of the experiment. Consequently, instead of a human operator, an OER is used to manipulate the master. The OER comprises a controller that allows us to achieve a desired SOP level while ensuring the non-passivity of the OER. In our experimental setup, the OER is a Phantom Omni and is coupled to the master robot as depicted in Fig. 10.

For simulating non-passive behavior by the OER, the OER is programmed to follow a sinusoidal position trajectory. In this way, the OER acts as a human operator who internationally moves the master. Internally, the OER has a proportional-derivative control controller so that its end-effector follows the pre-programmed trajectory. After the experiment with the OER coupled to the master is finished and all data is collected, the SOP (parameter η) is identified using Definition 4. As depicted in Figure 4, the input and output of the one-port network OER are the contact force and the velocity of the masters end-effector, respectively. The mechanical coupling of the OER to the masters end-effector provides us with the measurement of the contact force (using the force sensor) and end-effector velocity (using the Phantom Premiums position sensor). Therefore, we have all of the measurements of all signals present in Definition 4, and η can be found.

6.2.2. PEB architecture

The teleoperation system of Fig. 10 was controlled using a PEB controller. Two sets of controller gains were used: (a) $k_{p_m} = 10$, $k_{v_m} = 2$, $k_{p_m} = 10$ and $k_{v_m} = 2$, and (b) $k_{p_m} = 30$, $k_{v_m} = 2$, $k_{p_m} = 10$ and $k_{v_m} = 2$. In a separate experiment, the SOP of the OER was identified to be $\eta = 0.745$. Based on this non-passivity, the stability condition of the (PEB, INP) of Table 2 is checked for the two controller gain

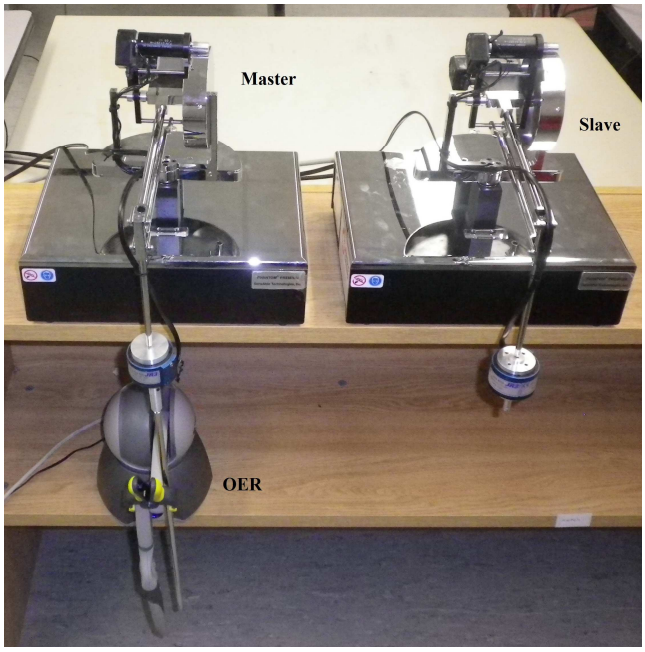

Figure 10. Block diagram model of the OER connected to the master robot via a flexible link.

sets. The stability condition for passive terminations, i.e., the (PEB, Passive) entry of Table 2, identifies the system with the first set of control gains as stable and with the second set of gains as unstable. However, both sets of control gains make the system become unstable in practice. The (PEB, INP) condition of Table 2 truly identifies both of the cases as unstable, which is in agreement with practice.

7. Conclusions and Future Work

Conventional stability analysis for two-port network systems relies on the assumption that the one-port network terminations for the two-port network are passive. In the context of bilateral teleoperation systems, where the terminations are the human operator and the environment, this assumption is less than accurate. As a result, the conventional stability analysis will be either invalid (when a termination is non-passive) or overly conservative (when a termination is strictly passive). In this paper, a powerful stability analysis tool has been developed based on complex-plane Mobius transformations of the termination impedance. The new stability criterion is able to give accurate assessment of (or conditions) for coupled two-port network stability in the presence of a non-passive termination when the conventional stability analysis may fail to identify potential instability. Conversely, the new stability criterion can provide more flexibility in control design in the presence of a strictly-passive termination and, therefore, help to achieve transparency improvement. Although the resulting stability conditions are valid for any two-port network, they are applied to PEB-controlled and DFR-controlled bilateral teleoperation systems and are tested both in simulations and experiments. In the future, the proposed approach can be extended to cases where both terminations of a two-port network are non-passive or strictly-passive. For example, a non-passive human operator may teleoperate a robot interacting with a non-passive (e.g., a beating heart) or a strictly-passive environment (e.g., any environment modeled as a mass-spring-damper). Another useful direction is to extend the approach presented here to multi-port network systems, which represent multilateral haptic teleoperation systems, that possibly also involve multi-DOF robots (Li et al. (2014)).

References

Adams, R., Hannaford, B., 1999. Stable haptic interaction with virtual environments. IEEE Transactions on Robotics and Automation 15 (3), 465–474.

Adams, R., Hannaford, B., January 2002. Control law design for haptic interfaces to virtual reality. IEEE Transactions on Control Systems Technology 10 (1), 3–13.

Aliaga, I., Rubio, A., Sanchez, E., January 2004. Experimental quantitative comparison of different control architectures for master-slave teleoperation. IEEE Transactions on Control Systems Technology 12 (1), 2–11.

Anderson, R., Spong, M., 1989. Bilateral control of teleoperators with time delay. IEEE Transactions on Automatic Control 34 (5), 494 –501.

Aziminejad, A., Tavakoli, M., Patel, R., Moallem, M., 2008. Transparent time-delayed bilateral teleoperation using wave variables. IEEE Transactions on Control Systems Technology 16 (3), 548–555.

Chopra, N., Spong, M. W., Lozano, R., 2008. Synchronization of bilateral teleoperators with time delay. Automatica 44 (8), 2142–2148.

Dolan, J., Friedman, M., Nagurka, M. L., 1993. Dynamic and loaded impedance components in the maintenance of human arm posture. IEEE Transactions on Systems, Man and Cybernetics 23 (3), 698–709.

Dyck, M., 2013. Measuring the dynamic impedance of the human arm. Master's thesis, University of Alberta, Edmonton, Alberta, Canada.

Dyck, M., Jazayeri, A., Tavakoli, M., 2013. Is the human operator in a teleoperation system passive? In: Proceedings of the IEEE World Haptics Conference 2013. Daejeon, Korea.

Haddadi, A., Hashtrudi-Zaad, K., 2010. Bounded-impedance absolute stability of bilateral teleoperation control systems. IEEE Transactions on Haptics 3 (1), 15 –27.

Haddadi, A., Hashtrudi-Zaad, K., 2012. Robust stability of teleoperation systems with time delay: A new approach. IEEE Transactions on Haptics (99).

Hannaford, B., Wood, L., 1989. Performance evaluation of a 6 axis high fidelity generalized force reflecting teleoperator. In: Proceedings of JPL/NASA Conference on Space Telerobotics. Pasadena, CA, pp. 89–97.

Hashtrudi-Zaad, K., Salcudean, S. E., 2001. Analysis of control architectures for teleoperation systems with impedance/admittance master and slave manipulators. The International Journal of Robotics Research 20 (6), 419–445.

Haykin, S., 1970. Active Network Theory. Addison-Wesley, Reading, MA.

Hill, D., Moylan, P., 1977. Stability results for nonlinear feedback systems. Automatica 13 (4), 377–382.

Hill, J. W., Jensen, J. F., 1998. Telepresence technology in medicine: Principles and applications. Proceedings of the IEEE 86 (3), 569–80.

Hirche, S., Matiakis, T., Buss, M., 2009. A distributed controller approach for delay-independent stability of networked control systems. Automatica 45 (8), 1828–1836.

Hogan, N., 1989. Controlling impedance at the man/machine interface. In: Proceedings of IEEE International Conference on Robotics and Automation. pp. 1626–1631 vol.3.

Hokayem, P. F., Spong, M. W., 2006. Bilateral teleoperation: An historical survey. Automatica 42 (12), 2035 – 2057.

Isidori, A., 1999. Nonlinear control systems II. Vol. 2. Springer Verlag, London, UK.

Jazayeri, A., Dyck, M., Tavakoli, M., 2013. Stability analysis of teleoperation systems under strictly passive and non-passive operator. In: Proceedings of the IEEE World Haptics Conference 2013. Daejeon, Korea.

Jazayeri, A., Tavakoli, M., 2012a. A passivity criterion for sampled-data bilateral teleoperation systems. IEEE transactions on Haptics (2012).

Jazayeri, A., Tavakoli, M., 2012b. Revisiting Llewellyns absolute stability criterion for bilateral teleoperation systems under non-passive operator or environment. In: Proceedings of the 2012 IEEE/RSJ International Conference on Intelligent Robots and Systems (IROS). Vol. 1. Vilamoura, Portugal, pp. 70–75.

Jazayeri, A., Tavakoli, M., 2013. Absolute stability analysis of sampled-data scaled bilateral teleoperation systems. Control Engineering Practice 21 (8), 1053–1064.

Khalil, H., 2001. Nonlinear Systems, 3rd Edition. Prentice Hall, Upper Saddle River, NJ, USA.

Kim, J., Chang, P., Park, H., 2013. Two-channel transparency-optimized control architectures in bilateral teleoperation with time delay. IEEE Transactions on Control Systems Technology 21 (1), 40–51.

Ku, W. H., 1963. Stability of linear active nonreciprocal n-ports. Journal of the Franklin Institute 276 (3), 207–224.

Lawrence, D. A., 1993. Stability and transparency in bilateral teleoperation. IEEE Transactions on Robotics & Automation 9, 624–637.

Lee, D., Spong, M., April 2006. Passive bilateral teleoperation with constant time delay. IEEE Transactions on Robotics 22 (2), 269 –281.

Levinson, N., Redheffer, R. M., 1970. Complex Variables. McGraw-Hill, Mishawaka, IN, USA.

Li, J., Tavakoli, M., Huang, Q., 2014. Absolute stability of multi-dof multilateral haptic systems. IEEE Transactions on Control Systems Technology 22 (6), 2319–2328.

Li, J., Tavakoli, M., Mendez, V., Huang, Q., 2013. Conservatism of passivity criteria for stability analysis of trilateral haptic systems. In: Proceedings of the IEEE World Haptics Conference 2013. Daejeon, Korea.

Llewellyn, F. B., 1952. Some fundamental properties of transmission systems. Proceedings of the IRE 40 (3), 271 –283.

Lozano, R., Maschke, B., Brogliato, B., Egeland, O., 2007. Dissipative Systems Analysis and Control: Theory and Applications. Springer-Verlag New York, Inc., Secaucus, NJ, USA.

Marquez, H., 2003. Nonlinear Control Systems: Analysis and Design. Wiley-Interscience, Hoboken, NJ, USA.

Matiakis, T., Hirche, S., Buss, M., 2009. Control of networked systems using the scattering transformation. IEEE Transactions on Control Systems Technology 17 (1), 60–67.
Niemeyer, G., Slotine, J. J. E., 2004. Telemanipulation with time delays. International Journal of Robotics Research 23 (9), 873–890.
Nuno, E., Basanez, L., Ortega, R., 2011. Passivity-based control for bilateral teleoperation: A tutorial. Automatica 47 (3), 485–495.
Park, K., , Chang, P. H., 2011. Stochastic estimation of human shoulder impedance with robots: An experimental design. In: Proceedings of the IEEE International Conference on Rehabilitation Robotics. Vol. 2011. pp. 1–8.
Polat, I., Scherer, C., 2012. Stability analysis for bilateral teleoperation: An IQC formulation. IEEE Transactions on Robotics 28 (6), 1294–1308.
Rodriguez-Seda, E. J., Spong, M. W., 2009. A time-varying wave impedance approach for transparency compensation in bilateral teleoperation. In: IEEE/RSJ International Conference on Intelligent Robots and Systems IROS. pp. 4609–4615.
Sepulchre, R., Jankovic, M., Kokotovic, P. V., 2012. Constructive nonlinear control, 1st Edition. Springer, London, UK.
Slotine, J., Li, W., 1991. Applied nonlinear control. Prentice-Hall Englewood Cliffs, NJ.
Spong, M., Vidyasagar, M., 2008. Robot Dynamics and Control. John Wiley & Sons.
Tavakoli, M., Aziminejad, A., Patel, R., Moallem, M., December 2007. High-fidelity bilateral teleoperation systems and the effect of multimodal haptics. IEEE Transactions on Systems, Man and Cybernetics – Part B 37 (6), 1512–1528.
Tsuji, T., Morasso, P. G., Goto, K., Ito, K., 1995. Human hand impedance characteristics during maintained posture. Biological cybernetics 72 (6), 475–485.
van der Helm, F. C., Schouten, A. C., de Vlugt, E., Brouwn, G. G., 2002. Identification of intrinsic and reflexive components of human arm dynamics during postural control. Journal of neuroscience methods 119 (1), 1–14.
van der Schaft, A., 1999. L2-Gain and Passivity in Nonlinear Control, 2nd Edition. Springer-Verlag New York, Inc., Secaucus, NJ, USA.
Willaert, B., Corteville, B., Reynaerts, D., Van Brussel, H., Vander Poorten, E., 2011. A mechatronic analysis of the classical position-force controller based on bounded environment passivity. The International Journal of Robotics Research 30 (4), 444–462.
Yan, J., Salcudean, S., 1996. Teleoperation controller design using h_∞-optimization with application to motion-scaling. IEEE Transactions on Control Systems Technology 4 (3), 244–258.

Appendix A. Proof of Theorems

Theorem 1

Proof. The rectangular shape in the z_2 plane (Fig. 3-a) consists of four lines of $\mathrm{Re}z_2 = -a$, $\mathrm{Re}z_2 = b$, $\mathrm{Im}z_2 = c$ and $\mathrm{Im}z_2 = -d$. Each of these four lines will be transformed to a circle in the Z_{a1} plane. In the following, in Step 1 the mapping of the vertical line $\mathrm{Re}z_2 = -a$ is found to be (8). Then, in Step 2, the mapping of the vertical line of $\mathrm{Re}z_2 = b$ is found and it is shown to be inside and tangent to the circle of (8). Finally, in Step 3 the mappings of the two horizontal lines are found and the region inside the rectangles is transformed.

Step 1:

Let us consider the vertical line of $\mathrm{Re}z_2 = -a$. The Mobius transformation (7) from z_2 plane into Z_{a1} plane is split to three transformations, namely a linear transformation ($\zeta_1 = z_2 + Z_{22}$), an inversion ($\zeta_2 = 1/\zeta_1$) and another linear transformation ($\zeta_3 = Z_{11} - Z_{12}Z_{21}\zeta_2$) Levinson and Redheffer (1970).

The three transformations are considered separately:

1. The first transformation is a linear transformation as $\zeta_1 = z_2 + Z_{22}$ that translates the LHP to the right side by the real part of Z_{22}, i.e. $R_{22} - a$ (Fig. A.11-b). The resulting line is expressed as $\mathrm{Re}\{\zeta_1\} = (R_{22} - a)$, which can be converted to the general circle/line formulation as $\zeta_1 + \bar{\zeta_1} = 2(R_{22} - a)$ (i.e. $A = 0$, $B = 1$ and $C = -2(R_{22} - a)$).
2. The second transformation is an inversion $\zeta_2 = 1/\zeta_1$. Substitution of the definition of the new transformation into result of step 1 reads as $1/\zeta_2 + 1/\bar{\zeta_2} = 2(R_{22} - a)$, which can be expressed in the general form of $-2(R_{22} - a)\zeta_2\bar{\zeta_2} + \zeta_2 + \bar{\zeta_2} = 0$(i.e. $A = -2(R_{22} - a)$, $B = 1$ and $C = 0$). This is an equation for a circle and hence this is a circle $\mathcal{C}(1/2(R_{22} - a), 1/2(R_{22} - a))$ (Fig. A.11-c). It should be noted that $R_{22} - a$ has to be positive because the vertical line in Fig. A.11b must be in the RHP.
3. The third transformation is $\zeta_3 = Z_{11} - Z_{12}Z_{21}\zeta_2$. Similar to the first transformation, the third transformation is a linear transformation (Fig. A.11-d). For this transformation the magnifying factor is $Z_{12}Z_{21}$ and translation is Z_{11}. Therefore, the circle will be expanded or contracted by factor of and $Z_{12}Z_{21}$ and the radius becomes $r_o = \frac{|Z_{12}Z_{21}|}{2(R_{22} - a)}$ and the centre of the circle will be translated to

$c_o = Z_{11} - \frac{Z_{12}Z_{21}}{2(R_{22}-a)}$. The latter shows that a region expressed as $\mathrm{Re}z_2 \geq -a$ is mapped to a region inside a disc express as in (8).

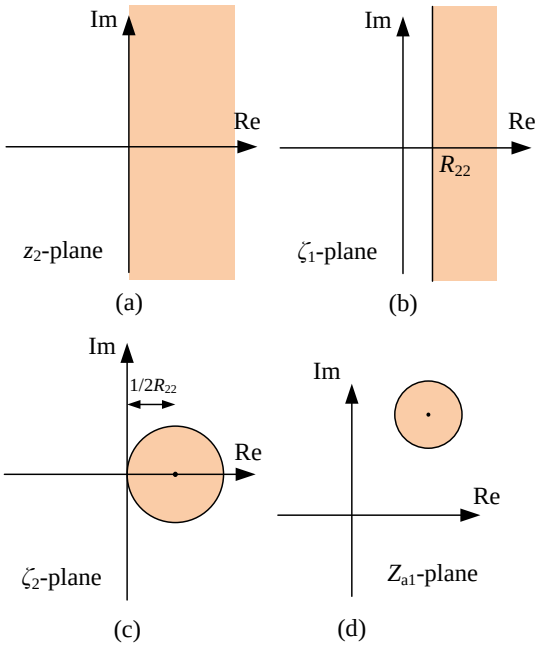

Figure A.11. The Mobius transformation has been split into three transformations: from (a) to (b) is a linear transformation (horizontal translation), from (b) to (c) is an inversion, and from (c) to (d) is another linear transformation with expansion/contraction in addition to a translation.

Step 2:

Similar to Step 1, it is easy to show that the vertical line of $\mathrm{Re}z_2 = b$ is transformed to a circle of (9). In the following it is shown that the circle of (9) is enclosed by the circle of (9) and also the two circles are tangent at the furthest point from the origin. Consequently, the area between the two vertical lines of $\mathrm{Re}z_2 = -a$ and $\mathrm{Re}z_2 = b$ is transformed to a cresent as shown in Fig. A.12.

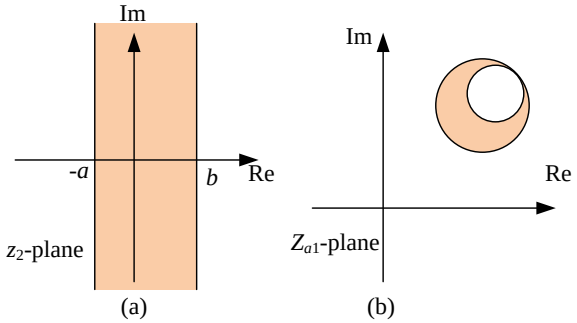

Figure A.12. In analysis of the strip-like impedances the strip in the z_2-plane (a) is mapped to a rotated crescent in the Z_{a1}-plane (b).

In the following, it is proved that the circle corresponding to $\mathrm{Re}z_2 = b$ is entirely inside the circle corresponding to $\mathrm{Re}z_2 = -a$. The two circles of (8) and (9) resulted from expansions/contractions term $Z_{12}Z_{21}$ followed by a translation by Z_{11} in the Z_{a1}-plane. Consequently, as depicted in Fig. A.13-a, an extension of the line connecting the centres of these two circles ($\overline{t_a t_b}$) goes through the origin. Another

conclusion is that the length of the line segment between the centres of the two circles, i.e., $|\overline{t_a t_b}|$, is identical to the differences between to the radii of the two circles (i.e., $|{}^a r_o - {}^b r_o|$). Therefore, as shown in Fig. A.13-a, the two circles must be tangent at their farthest points from the origin. Additionally, changing the bounds on the real part of z_2 will result in the circles shown in Fig. A.13-b. As the real value of z_2 is allowed to increase, the radius of the smaller circles decreases. Also, as the real value of z_2 is allowed to decrease further into the negative values, the radius of the larger circles increases (not shown in Fig. A.13-b).

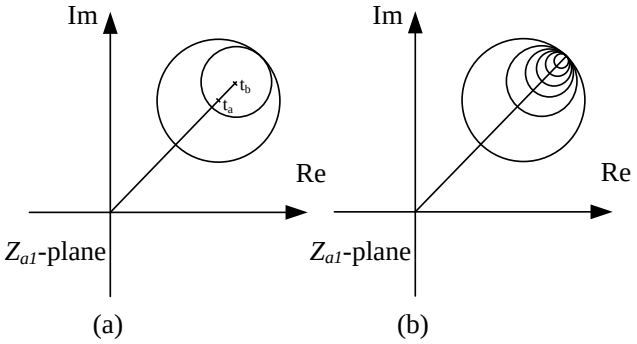

Figure A.13. The vertical lines in the z_2-plane are mapped to circles in the Z_{a1}-plane. The vertical line at $\mathrm{Re}\, z_2 = -a$ is mapped to the larger circle in the Z_{a1}-plane while the vertical line at $\mathrm{Re}\, z_2 = b$ is mapped to the smaller circle (a). As the real value of z_2 is allowed to increase (i.e., larger b), the radius of the smaller circle decreases while the circles still share the same tangent point.

Step 3:

In this step of the proof, it is shown that the horizontal lines of $\mathrm{Im} z_2 = c$ and $\mathrm{Im} z_2 = -d$ are transformed to circles of (10) and (11). Let us consider the horizontal line of $\mathrm{Im} z_2 = c$.

Similar to Step 1, the Mobius transformation (7) is split into three transformations, in which the first and the third are linear transformations and the second transformation is an inversion. The line $\mathrm{Im} z_2 = c$ is expressed as $z_2 + \bar{z}_2 = 2cj$ and the definition of the first transformation $\zeta_1 = z_2 + Z_{22}$ is substituted to yield the resulting line in ζ_1-plane as $\zeta_1 - \bar{\zeta_1} = 2cj + 2I_{22}$, where $I_{22} = \mathrm{Im}\{Z_{22}\}$. If it is assumed that $I_{22} + c \geq 0$, substituting the definition of the second transformation $\zeta_2 = 1/\zeta_1$ one can find the transformed the circle in the ζ_2 plane to be $-(2c + 2I_{22})\zeta_2\bar{\zeta_2} + j\zeta_2 - j\bar{\zeta_2} = 0$, which has the general circle/line formulation with $A = -(2c + 2I_{22})$, $B = -j$ and $C = 0$. The equation in the ζ_2-plane is $\mathcal{C}(1/(2c + 2I_{22}), -j/(2c + 2I_{22}))$, which is a circle below the origin but tangent to the real axis at the origin. The third transformation $\zeta_3 = Z_{11} - Z_{12}Z_{21}\zeta_2$ bears a translation of Z_{11}, mirrors the circle, expands the circle with expansion factor of $|Z_{12}Z_{21}|$ and finally rotates the circle around Z_{11} about the angle of $Z_{12}Z_{21}$. The resulting circle in the Z_{a1}-plane is circle of (10).

As depicted in Fig. A.14 by increasing the imaginary level c in z_2-plane makes the smaller circles in Z_{a1}-plane, where all of the circles have a tangent point in common at Z_{11}. The region corresponding the region lower than the upper limit of $\mathrm{Im} z_2 = c$ in the z_2-plane is transformed to the region outside of the disc expressed by (10) in the Z_{a1}-plane (see Fig. A.15).

Similar to the above mapping for $\mathrm{Im} z_2 = c$, it is easy to show that the mapping of the horizontal line of $\mathrm{Im} z_2 = -d$ is (11). The assumption of $I_{22} + c \geq 0$ is also replaced by $I_{22} - d \leq 0$.

Note that by increasing the limit on the imaginary part of the upper limit to infinity and decreasing the lower limit to minus infinity, the mapped region in the Z_{a1}-plane becomes the entire plane due to the fact that the radii of the circles decreases as the limit are going further from the real axis.

Combining the transformation of the four lines of Step 1, 2 and 3 the rectangle of Fig. 3-a in the z_2 plane is transformed to the portion of a crescent, where the two sides of the crescent are excluded from the region as shown in Fig. 3-b expressed with the circles of (8)-(11) in the Z_{a1} plane. □

Theorem 2

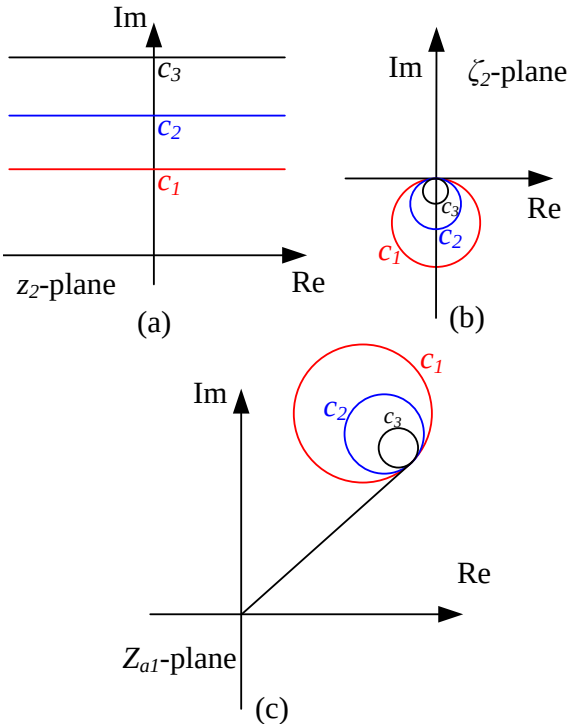

Figure A.14. The horizontal lines in the z_2-plane are transformed into circles in the Z_{a1}-plane. As the horizontal line moves up, the radius of the circles decreases. Yet, all of the circles are tangent at one point.

Proof. As explained in the proof of Theorem 1 the Mobius transformation (7) is split to three transformations. (1) a linear transformation of $\zeta_1 = z_2 + Z_{22}$, (2) an inversion $\zeta_2 = 1/\zeta_1$, and (3) a linear transformation $\zeta_3 = Z_{11} - Z_{12}Z_{21}\zeta_2$. Lines or circles are expressed in the formulation in the complex plane.

The border of the disc is $\mathcal{C}(M, 0)$ in the z_2-plane and is expressed as $z_2\bar{z_2} = M^2$ in the circle/line formulation. From the first transformation of $z_2 = \zeta_1 - Z_{22}$, substitution of z_2 is a shifted circle expressed as $\zeta_1\bar{\zeta_1} - \bar{Z_{22}}\zeta_1 - Z_{22}\bar{\zeta_1} + |Z_{22}|^2 - M^2 = 0$, which is a circle in the general expression with $A = 1$, $B = -\bar{Z_{22}}$ and $C = |Z_{22}|^2 - M^2$. The second transformation is substituted as $\zeta_1 = 1/\zeta_2$. After simplification the resulting shape is $1 - \bar{Z_{22}}\bar{\zeta_2} - Z_{22}\zeta_2 + (|Z_{22}|^2 - M^2)\zeta_2\bar{\zeta_2} = 0$. Now, this shape can be either a circle or a line depending whether $|Z_{22}| = M$ or not. If $|Z_{22}| \neq M$ the mapped shape in the ζ_2-plane is a circle otherwise it is a line. These two cases are considered separately below.

- If $|Z_{22}| \neq M$, resulting shape is a circle $\mathcal{C}(\frac{M^2}{||Z_{22}|^2 - M^2|}, \frac{Z_{22}}{|Z_{22}|^2 - M^2})$. The third transformation shift this circle to another circle $\mathcal{C}(\frac{|Z_{12}Z_{21}|M^2}{||Z_{22}|^2 - M^2|}, \frac{-Z_{22}Z_{12}Z_{21}}{|Z_{22}|^2 - M^2} + Z_{11})$ and the mapped region is inside this circle (see Fig. A.16-b).
- If $|Z_{22}| = M$, the result of the second transformation is a line $1 - \bar{Z_{22}}\bar{\zeta_2} - Z_{22}\zeta_2 = 0$. This line is vertical only if the coefficient of $\bar{\zeta_2}$ is zero, which requires that Z_{22} to have no imaginary part, and otherwise the resulting region is a rotated and shifted half plane and hence there is no condition in which guarantees the region to be entirely in the RHP. With the assumption of $\mathrm{Im}Z_{22} = 0$, the mapped region in ζ_2-plane is a vertical line at $\zeta_2 = 1/2R_{22}$. The third transformation shifts this vertical line to $R_{11} - \mathrm{Im}\{Z_{12}Z_{21}\}/2R_{22}$. Therefore, the mapped region in the Z_{a1}-plane is the right hand side of this vertical line (see Fig. A.16-c).

□

Theorem 4

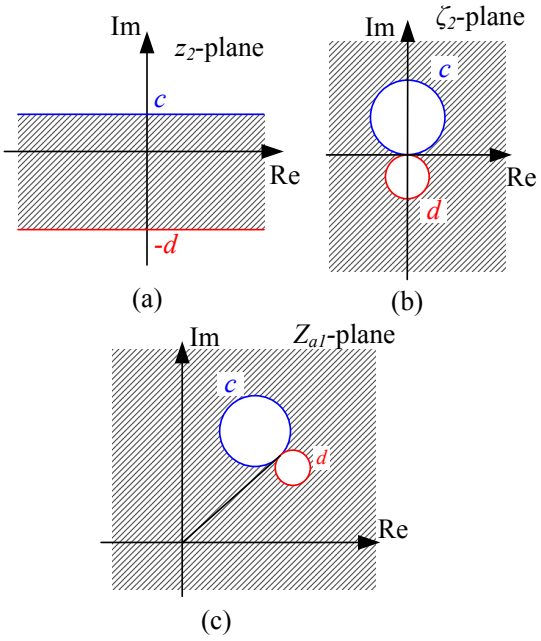

Figure A.15. The area between the two horizontal lines in the z_2-plane are transformed into the hatched area in Z_{a1}-plane.

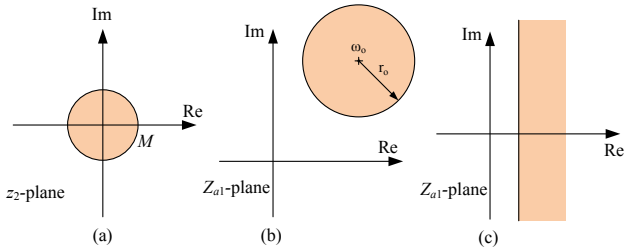

Figure A.16. (a) a disc in the z_2-plane inside $\mathcal{C}(M,0)$, (b) if $|Z_{22}| \neq M$, the mapped region is also a disc in the Z_{a1}-plane, (c) if $|Z_{22}| = M$, the mapped region is a shifted RHP.

Proof. Conditions (i) and (ii) are necessary conditions for ensuring positive realness of Z_{11} and Z_{22} in zero-impedance conditions for ports 2 and 1, respectively. Let us consider the third condition of Theorem 4. As shown in Fig. 1-b, the two-port network is connected to a passive impedance z_2 and the input impedance seen from the other port is assumed to be Z_{a1}. The two-port network will be absolutely stable if Z_{a1} is passive as well. The driving-point impedance Z_{a1} is expressed based on the two-port network impedance parameters Z_{ij}'s and the termination impedance z_2 as in (7).

The borderline of passivity in the z_2 complex plane is a vertical line at $-a$. If $\mathrm{Re}Z_{22} \geq a$, and for similar reason $\mathrm{Re}Z_{11} \geq 0$, Theorem 1 applies with $b = \infty$, $c = \infty$ and $d = \infty$. The passive region is mapped to a disc inside of $\mathcal{C}(|Z_{12}Z_{21}|/(2(R_{22}-a)), Z_{11} - Z_{12}Z_{21}/(2(R_{22}-a)))$. The condition for passivity of the driving-point impedance Z_{a1} is that this disc with radius of r_o and centre of c_o must be entirely in the RHP, i.e., $\mathrm{Re}c_o - r_o \geq 0$. Thus, the absolute stability becomes

$$\frac{2\mathrm{Re}Z_{11}\mathrm{Re}Z_{22} - \mathrm{Re}\{Z_{12}Z_{21}\} - |Z_{12}Z_{21}|}{2(R_{22}-a)} \geq 0 \tag{A.1}$$

This completes the proof. □